HHS Public Access

Author manuscript

Adv Mater. Author manuscript; available in PMC 2024 February 01.

Published in final edited form as:

Adv Mater. 2023 February ; 35(5): e2207335. doi:10.1002/adma.202207335.

Extracellular Matrix Secretion Mechanically Reinforces Interlocking Interfaces

Alec McCarthy,
Department of Surgery – Transplant and Mary & Dick Holland Regenerative Medicine Program, University of Nebraska Medical Center, Omaha, NE, 68198, USA

Navatha Shree Sharma,
Department of Surgery – Transplant and Mary & Dick Holland Regenerative Medicine Program, University of Nebraska Medical Center, Omaha, NE, 68198, USA

Phil A. Holubeck,
Department of Surgery – Transplant and Mary & Dick Holland Regenerative Medicine Program, University of Nebraska Medical Center, Omaha, NE, 68198, USA

Demi Brown,
Department of Surgery – Transplant and Mary & Dick Holland Regenerative Medicine Program, University of Nebraska Medical Center, Omaha, NE, 68198, USA

Rajesh Shah,
Spectro Coating Corporation, Flock Coatings & Short Cut Fibers, Leominster, MA, 01453, USA

Daniel McGoldrick,
Department of Computer Science, School of Computing & Design, California State University - Monterey Bay, Seaside, CA, 93933 USA

Johnson V. John,
Department of Surgery – Transplant and Mary & Dick Holland Regenerative Medicine Program, University of Nebraska Medical Center, Omaha, NE, 68198, USA

S M Shatil Shahriar,
Department of Surgery – Transplant and Mary & Dick Holland Regenerative Medicine Program, University of Nebraska Medical Center, Omaha, NE, 68198, USA

Jingwei Xie[*]
Department of Surgery – Transplant and Mary & Dick Holland Regenerative Medicine Program, University of Nebraska Medical Center, Omaha, NE, 68198, USA; Department of Mechanical and Materials Engineering, University of Nebraska Lincoln, Lincoln, NE, 68588, USA

Abstract

Drawing inspiration for biomaterials from biological systems has led to many biomedical innovations. One notable bioinspired device, Velcro, consists of two substrates with interlocking

[*] jingwei.xie@unmc.edu (J. Xie).

Supporting Information
Experimental details are included in the Supporting Information.

ability. Generating reversibly interlocking biomaterials is an area of investigation, as such devices could allow for modular tissue engineering, reversibly interlocking biomaterial interfaces, or friction-based coupling devices. Here, we report a biaxially-interlocking interface generated using electrostatic flocking. Two electrostatically flocked substrates are mechanically and reversibly interlocked with the ability to resist shearing and compression forces. An initial high-throughput screen of polyamide flock fibers with varying diameters and fiber lengths was conducted to elucidate the roles of different fiber parameters on scaffold mechanical properties. After determining the most desirable parameters via weight scoring, polylactic acid (PLA) fibers were used to emulate the ideal scaffold for in vitro use. PLA flocked scaffolds were populated with osteoblasts and interlocked. Interlocked flocked scaffolds improved cell survivorship under mechanical compression and sustained cell viability and proliferation. Additionally, the compression and shearing resistance of cell-seeded interlocking interfaces increased with increasing extracellular matrix deposition. The introduction of extracellular matrix-reinforced interlocking interfaces may serve as binders for modular tissue engineering, act as scaffolds for engineering tissue interfaces, or enable friction-based couplers for biomedical applications.

Graphical Abstract

This work reports a bioinspired interlocking interface produced by electrostatic flocking. Such an interface can sustain cell growth and the perpendicularly aligned flocked fibers can mitigate cell death caused by compression. In addition, the secreted extracellular matrix from seeded cells significantly enhances the mechanical properties of the interface.

Keywords

interlocking interface; electrostatic flocking; extracellular matrix; compression shielding; mechanical reinforcement

1. Introduction

For decades, engineers and scientists have turned to nature for design inspiration, resulting in the birth of biomimicry and biomimetics engineering.[1-3] Specifically, many biomedical engineers and material scientists have focused on emulating naturally occurring micro and nanostructures to generate functional materials. These efforts have led to the development of many materials, of which dry adhesives (i.e., based on Gecko pads) and interlocking materials (i.e., based on burrs) rely upon mechanical interlocking to resist pull-off or shearing forces.[4-7] The majority of dry adhesives draw inspiration from hook-and-loop, suction pad, or shape-based (i.e., male-to-female) interlocking and report a variety of applications.[8-11] Arguably one of the most reliably reversibly interlocking devices, Velcro, employs a simple hook-and-loop design and has repeated interlockability, with shear resistance owed in part to friction and finite material displacement.[12] Though several studies have explored interlocking interfaces for different biomedical applications (i.e., modular tissue engineering, tissue interlocking, wound closure), they remain largely underexplored.[13-16] Often, these interfaces are created with a one-step design approach (often using polydimethylsiloxane (PDMS)) to address a single mechanical feature (i.e., shearing resistance, compression resistance, etc). Modular tissue engineering focuses on

building complex anatomical structures by developing cell or tissue-specific building blocks that can be interlocked, stacked, or mechanically connected.[17] In order to facilitate modular tissue engineering with mechanically-interlocking interfaces, interlocked scaffolds should be biocompatible, retain high porosities to facilitate cell and nutrient migration, and should protect cells from mechanical stresses expected from the anatomical structures being emulated.[17-19] One may expect that a mechanically interlocked biomaterial populated with cells will be the recipient of cell-secreted extracellular matrix (ECM).[20, 21] To this end, interlocked scaffolds that work synergistically with the ECM and cells may improve outcomes in modular tissue engineering, especially in applications where two dissimilar tissues are to be mechanically interlocked (i.e., muscle-to-tendon, cartilage-to-bone, and tendon-to-bone).

Noting the lack of material flexibility and approaches to design an interlocking scaffold that synergistically utilizes native ECM deposition, we report a novel, electrostatic flocking-based interlocking and extracellular matrix-reinforced biomaterial created to withstand shearing and compressive loads in biological conditions and improve cell survivorship during mechanical deformations (Figure 1). In this case, the flock fibers lack the hook-and-loop design of Velcro, and therefore retain ease of reversibility when removing via pull-off. The ability to reversibly interlock allows for adjustment and an additional degree of freedom with movement. In order to rationally determine ideal interlocking scaffold characteristics, we conducted a high-throughput screen of flocked scaffolds with varying fiber lengths and diameters using Nylon-6,6 as a model polymer and assessed several key scaffold parameters including morphological homogeneity, porosity, abrasion resistance, compressive strength, and shearing resistance. After identification of an ideal Nylon-6,6 scaffold, a polylactic acid (PLA) and PDMS-based interlocked scaffold produced by electrostatic flocking was modeled and evaluated as an interlocking interface under in vitro conditions. After emulating an ideal reversibly interlocking scaffold, we demonstrated several key findings: *i)* interlocked scaffolds can support and facilitate cell proliferation within pores and between interlocking fibers; *ii)* the anisotropy of the scaffold protects cells from compression-related cell death pathways; and *iii)* the mechanical strengths of interlocked scaffolds are enhanced by the secretion of the ECM from seeded cells.

2. Results and Discussion

A high-throughput screen using Nylon-6,6 with different diameter and length flock fibers was first conducted to elucidate the impact of fiber morphology on scaffold mechanical properties. Nylon-6,6 was selected as a model polymer due to its similar properties to PLA, ease of production, and low cost given the high number of fibers needed for this study. Briefly, a woven substrate was coated with an industrial grade adhesive and electrostatically flocked with Nylon-6,6 fibers. For the purpose of the high-throughput screen, a low-cost woven Nylon-6,6 substrate was utilized. The mechanics tested are impartial to the substrate used. Table 1 outlines the different fiber types that composed each flock scaffold. We generally classified fibers into four groups based on their decitext (dTex) (25, 15, 6, 3 & 1.5). Dtex is a metric unit used to measure continuous linear fibers and reports the mass in grams per 10,000 meters. Within each group, 4 different fiber lengths were fabricated (1500, 1000, 750, and 500 μm). Each fiber type was assigned a letter in alphabetical

order from highest dTex and increasing fiber length. For example, samples A-D all have dTex of 25 and increase in length from 500 μm to 1500 μm, while samples E-H have dTex of 15 and increase in length from 500 μm to 1500 μm. All fibers were imaged via scanning electron microscopy (SEM) and their characteristics were analyzed with ImageJ. The average diameters for Group 1 (A-D) (25 dTex), Group 2 (E-H) (15 dTex), Group 3 (I-L) (6 dTex) and Group 4 (M-P) (3 & 1.5 dTex) were measured at 51.67 ± 2.08 μm, 43.25 ± 1.30 μm, 27.63 ± 0.62 μm, 17.77 ± 1.88 μm, and 15.38 ± 0.88 μm in diameter. The importance of understanding and controlling flock fiber diameter is two-fold. First, studies into fiber-fiber interactions reveal that fiber diameter plays a role in fiber rigidity (and related finite displacement), friction interactions, fiber packing, and compressive resistance.[6, 22-24] Unlike previous studies, though, we sought to optimize the aspect ratio of fibers to achieve optimal compression and shearing resistance. Second, previous studies have not only shown the impact on fiber diameter for modulating cellular orientation[25], but also that fiber density affects infiltration of host cells and angiogenesis.[26] In addition to characterizing flock fiber morphologies, we examined the structures and fiber orientations of flocked surfaces using each fiber type with SEM (Figure S1a). Once SEM images were obtained, the ImageJ plugin OrientationJ was used to measure field tensors and generate an alignment histogram. Generally, scaffold anisotropy increased with decreasing fiber length, though fiber diameter did not have a significant impact on orientation. Fibers appeared straight with approximately +/− 20% of the desired length (Figure S1 b & c). Determining the packing density and quality of anisotropy are two important factors in estimating and understanding compressive resistance.[22,24,27] By measuring the Euclidean distance between neighboring fibers, it is possible to approximate the bulk structural porosity via 3D projection of fiber cross sections. Scaffolds were frozen and cross-sectional images were taken to calculate packing density using the ImageJ Delaunay Triangulation plugin (Figure S1 d & e).[22] We assume that scaffolds with larger average distances between neighbors are more porous. Since each scaffold was produced under the same flocking conditions, variations in fiber packing are related to only fiber morphology. Significant differences in Euclidean distance within ($p < 0.0001$, n = 8) and between groups ($p < 0.0001$, n = 16) were noted. Though no literature exists to ascertain an ideal aspect ratio for flocking, a general rule of thumb is 10:1 length: diameter for optimal flocking alignment. Summary data for fiber diameter and maximum orientation frequency is presented in Table 1 and Figure S1f. Table S1 and Figure S1g summarizes the average distance between fibers for each sample and group.

After characterizing the structures of each scaffold type, compression and shearing resistance tests were conducted at fixed rates. Shearing resistance (Figure 2a (representative graph of sample P)) was measured using a modified tensile test, where each side of the scaffold was fixed to an arm of the mechanical testing device. At the start of the modified tensile test, the scaffold was interlocked and at rest. A constant shearing force was applied until the two flocked layers were separated. Photographs of scaffolds during shearing tests were shown in Figure S2 a & Figure S3 a-c. While the fibers can interlock and resist shearing forces without cells or a transverse load, three conditions of transverse loads were tested: no load, a small load (~5 N), and a large load (~20 N) (Figure 2 b). For these tests, two clamps with varying clamp forces were applied normal to the fiber orientation. The rationale behind testing different transverse loads was the assumption that the depth of

interpenetrating fibers regulated the degree of interlocking. That is, higher transverse loads may facilitate deeper degrees of fiber penetration and improve the shearing resistance of the scaffolds. Scaffolds responded differentially to the degree of transverse load such that long and thick fibers had higher critical forces under no load (defined as the switch from static to kinetic friction), while shorter and thinner fibers had higher critical forces under higher transverse loads (due to fiber-fiber friction) (Figure 2 c-e). Compression testing consisted of applying a compressive load at a constant rate parallel to interlocked scaffolds for 4 cycles (Figure 2 f (representative graph of sample D, Figure S2 b, Figure S3 d-f). Compressive resistance decreased with decreasing fiber diameter. A summary of maximum compressive loads is given in Figure 2 g. Finally, abrasion resistance (mass loss) revealed an approximate 12-17% mass loss in samples from Group 1 (highest dTex) (Figure S4). This insight revealed that large diameters caused too much fiber loss during abrasion, largely due to the increased surface area subject to abrasive forces. After determining the compressive strength, shearing resistance, coefficient of kinetic friction, mass loss, and fiber density of each scaffold (Table S2), a weighted matrix was used to select the most optimal scaffold morphology. The weighted T-Score table (Table S3) revealed scaffold type O (1.5 dTex, 30 μm fiber length) was most optimal and was therefore emulated with a biocompatible polymer Poly($_L$-lactide) (PLA).

To evaluate the biological role interlocking flocked scaffolds may have in tissue engineering, we first verified the proper emulation of an ideal scaffold as determined by our weighted scoring or our high-throughput screen (Figure S5). Creation of PLA scaffolds with interlocking ability was verified *via* SEM (Figure S5 a & b). PLA was chosen as an ideal polymer due to its mechanical strength, biocompatibility, and ease of flocking.[28-30] The PLA fiber lengths and diameters closely emulated that of sample O, which was weighted as one of the three highest-scoring scaffolds. Additionally, the packing density and fiber diameter distribution of PLA scaffolds emulated those reported in sample O (Figure S5 d & e). Finally, to ensure cell viability, MC3T3-E1 cells were seeded on the PLA scaffolds and viability was measured at day 1, 3, 5, and 7, showing a significant increase in proliferation ($p < 0.0001$, n = 8) (Figure S5 f). Collagen staining at day 7 revealed pockets of collagen deposited in the immediate vicinity of cells (n = 3) (Figure S5 c).

After ascertaining the mechanical stability of the PLA scaffolds, we sought to determine whether the scaffolds could redistribute compressive loads away from seeded cells, thus improving cell survivorship during mechanical perturbation. A variety of cell death pathways are induced during mechanical compression of cells and thus, stress shielding is a desirable scaffold property.[31-35] We proposed a fiber bending mechanism that may impart small localized deformations on cells adhering to fibers, but alleviates large full-cell compression (Figure 3 a). Custom 3D-printed compression inserts (Figure 3 a) with verified stress transfer were first evaluated for any induction of cytotoxicity using a cell viability assay. It was found that, after directly culturing MC3T3-E1 cells with 3D printed compression inserts, viability insignificantly increased, yet remained above 90% viability after 24 and 48 h ($p = 0.827$, n = 8) (Figure 3 b). After ascertaining non-cytotoxicity of the compression insert, we applied different compressive loads (0, 0.6 kPa, 1.1 kPa, 2.8 kPa, and 5.5 kPa) to each well by exerting a defined force onto the cell culture inserts, which was directly seeded with MC3T3-E1 cells (no scaffolds). In this case, with viability expressed

as the absorbance normalized to cells under static culture conditions, we noted the first significant decrease in viability at 1.1 kPa of compressive load, which increased dramatically under 2.8 and 5.5 kPa (Figure 3 c). Based on the finding that viability significantly decreased after applying 1.1-2.8 kPa of compressive loads to the cells, we chose to apply 2 kPa of compressive load to cells in order to induce compressive cell death. Cells were either seeded on electrospun PLA nanofiber membranes or on flocked scaffolds and 2 kPa of compressive load was applied for 24 h. After 24 h, we measured viability, normalized to the highest average static culture optical density, and found that flocked scaffolds had a more significant protective effect than electrospun nanofiber membranes, but that static (no pressure applied) cultures in both electrospun nanofiber membranes and flocked scaffold groups showed the highest viability, as one may expect ($p < 0.001$, n = 8) (Figure 3 d). In this study, electrospun nanofiber membranes were used as controls for the following reasons. The electrospun nanofiber membranes were thick enough to have some mechanical “give”. That is, the material could absorb a small amount of the compressive load, which would allow for an even force to be exerted to the cells in the compressive field. In large part, these findings are consistent with those reported by Loening et al., who found a pressure-dependent reduction in viability.[31] By enabling fiber bending, flocked scaffolds redistribute otherwise apico-basal compressive loads that would trigger cell death.[35] This set of studies revealed a key finding. Compression-induced cell death can be mitigated by seeding cells in compression-resisting scaffolds. As such, flocked scaffolds rescued significantly more cells than electrospun membranes, as flocked scaffolds experienced an 8% reduction in viability while electrospun membranes experienced a 44% reduction after compression ($*p < 0.05$, $***p < 0.001$, n = 8). Taken together, flocked scaffolds demonstrated the ability to protect cells during mechanical compression, largely due to the scaffolds’ ability to resist compression from fiber bending.

Noting the ability to sustain cell proliferation and survivorship during mechanical perturbation, it was hypothesized that scaffolds would also experience an increase in mechanical strength with the proliferation of seeded cells and their secreted ECM. To investigate this, it was first critical to ascertain the deposition of ECM components. A long-term culture of MC3T3-E1 cells was carried over a 40-day period. MC3T3-E1 cells were chosen for demonstrating the proof-of-concept in this study. In addition, this was the first step to engineer tissue interfaces like bone-cartilage, bone-tendon, and bone-muscle. Confocal imaging of COL1A and DAPI revealed that the secretion of type I collagen was modest at day 10 and significantly increased between day 20, 30, and 40 (Figure 4 a). A variety of osteogenic genes were analyzed at baseline, day 10, 20, 30, and 40 to confirm that osteogenic differentiation could occur during culture with interlocked scaffolds. To this end, BMP7, RANKL, BSP, ALP, OCN, OPG, RUNX2, and Col1A were analyzed with PCR (Figure 4 b and Table S4). Each investigated gene significantly increased as a function of culture time except OPG, which exhibited insignificant changes between days 10 to 40. At day 0 (baseline), 10, 20, 30, and 40, scaffolds were subject to compression and shearing tests as above described ($p < 0.0001$, n = 8). The increase in collagen staining intensity and cell counts at different depths ascertain the penetration and proliferation of cells along the lengths of interlocked scaffolds. The changes in osteogenic markers further indicate that the 3D environment is capable of stimulating osteogenic differentiation.

Finally, to illustrate how an interlocked scaffold may synergistically function with exogenous or endogenous cells and ECMs, force curves for compression and shear resistance were measured for MC3T3-E1 cells-seeded interlocking scaffolds after culture for 10, 20, 30, and 40 days (Figure 5 a & b). Briefly, interlocked scaffolds seeded with MC3T3-E1 cells were taken directly from cell culture and positioned for either a shear or compression test as previously described in the high-throughput section of this study. It is widely accepted that collagen is a major contributor to ECM mechanical strength.[36, 37] In this case, we sought to understand how collagen deposition within the interlocked scaffold would affect the scaffold's overall mechanical properties. Collagen (COL1A) was quantified at day 10, 20, 30, and 40 days via hydroxyproline measurement, revealing an increase from roughly 60 μg/scaffold at day 10 to approximately 250 μg/scaffold by day 40 ($p < 0.0001$, n = 10) (Figure 5 c). Compression resistance increased by roughly 4 times ($p < 0.001$, n = 8) from baseline to day 40 and was highly correlated with increasing collagen content ($p < 0.0001$, n = 8) as confirmed by linear regression (Figure 5 a, c & d). Similarly, shearing resistance increased by roughly 10 times from baseline to day 40 ($p < 0.0001$, n = 8) and was closely correlated with increasing collagen content ($p < 0.0001$, n = 8) as confirmed by linear regression (Figure 5 b & e). Percent changes from baseline are noted in Figure 5 f & g. Notably, it appears shearing resistance is influenced to a higher degree by collagen content, likely due to the increase in the secreted type I collagen matrix securing the interlocked flocking fibers. This final set of experiments reveal several key findings. First, interlocked scaffolds seeded with MC3T3-E1 cells sustained significant ECM synthesis that, in turn, increased the bulk scaffold compression and shearing resistance. These results indicate that an interlocking scaffold is reinforced by ECM synthesis, likely by secreted type I collagen that interacts with the interlocked fibers in a synergistic and reinforcing manner. Second, gene expression crucial for osteogenic differentiation is maintained and confirmed. Taken together, the biomechanical basis for a novel interlocking scaffold that is reinforced by native collagen secretion is warranted. Such an interlocking scaffold could be potentially used for modular tissue engineering, engineering tissue interfaces (e.g., muscle-bone, tendon-to-bone, bone-cartilage, dermal-epidermal junction), and structured bioadhesive.

3. Conclusion

In summary, we have demonstrated the rational design of a novel interlocking interface that protects cells during mechanical compression and is mechanically reinforced via a synergistic mechanism with cells and their ECM secretion. We have revealed several key considerations for optimizing an electrostatically flocked interlocking interface based on a high-throughput mechanical screen of a variety of fiber characteristics. We have shown a biocompatible substitute consisting of PLA flocking fibers exhibiting similar morphological properties while retaining cell viability under culture conditions. When MC3T3-E1 cells were seeded on interlocked scaffolds and subject to otherwise lethal compressive loads, cell death was significantly mitigated by redistributing forces via fiber bending. We have also shown the ability of interlocking flocked interfaces to sustain MC3T3-E1 cell growth during the long-term culture and their ECM secretion serving to mechanically reinforce the interfaces as well as facilitating osteogenic differentiation. It is worth reiterating that,

without cells, flocked scaffolds demonstrate reversible interlocking. This alone may have implications in device development outside the scope of biomedical applications. However, when ECM is secreted, the interlocking effect is enhanced and becomes irreversible. As we further develop this material and approach a more Velcro-like design meant to interlock in all directions, tension will be examined other than shearing and compression. Future studies may also seek to investigate how fiber surface functionalization with peptides, short nanofibers/nanoparticles, and other biologics may influence the biological or mechanical properties of such scaffolds. Synergy between surface functionalization, bulk scaffold morphology, and biological activity can be further optimized and tailored for anatomy-specific applications. Further, studies investigating the addition of two dissimilar cell types to create a confluent interface may reveal the role this type of scaffold may have on interlocking distinct tissues types (i.e., cartilage-bone). This interlocking interface may serve as bonding site to connect different engineered tissues for modular tissue engineering. Such an interface could also be applied to mimic and model a variety of tissue interfaces and generate friction-based couplers.

Supplementary Material

Refer to Web version on PubMed Central for supplementary material.

Acknowledgements

This work was partially supported by startup funds from the University of Nebraska Medical Center (UNMC), National Institute of General Medical Science (NIGMS) and National Institute of Dental and Craniofacial Research (NIDCR) of the National Institutes of Health under Award Numbers P30GM127200, and R01DE031272, Congressionally Directed Medical Research Program (CDMRP)/Peer Reviewed Medical Research Program (PRMRP) FY19 W81XWH2010207, Nebraska Research Initiative grant, and NE LB606. The authors would like to acknowledge Sedighe Keynia and Wen Qian at the Nebraska NanoEngineering Research Core Facility. The authors would also like to acknowledge Spectro Coating and Claremont Flock for their help in preparing the large quantities of flocked fibers used in this work.

References

[1]. Xiang T, Hou J, Xie H, Liu X, Gong T, Zhou S, Nano Today 2020, 35, 100980.

[2]. Arzt E, Quan H, McMeeking RM, Hensel R, Prog. Mater. Sci 2021, 120, 100823.

[3]. Zhu M, Zhang F, Chen X, Small Structures 2020, 1, 2000045.

[4]. Chen C-M, Chiang C-L, Lai C-L, Xie T, Yang S, Adv. Funct. Mater 2013, 23, 3813.

[5]. Fiorello I, Tricinci O, Naselli GA, Mondini A, Filippeschi C, Tramacere F, Mishra AK, Mazzolai B, Adv. Funct. Mater 2020, 30, 2003380.

[6]. Pang C, Kim T, Bae WG, Kang D, Kim SM, Suh K-Y, Adv. Mater 2012, 24, 475. [PubMed: 22213515]

[7]. Seong M, Park H-H, Hwang I, Jeong HE, Coatings 2019, 9, 48.

[8]. Jiao J, Zhang F, Jiao T, Gu Z, Wang S, Adv. Sci 2018, 5, 1700787.

[9]. Su S, Wang S, Li L, Xie Z, Hao F, Xu J, Wang S, Guan J, Wen L, Matter 2020, 2, 1207.

[10]. Greiner C, Arzt E, del Campo A, Adv. Mater 2009, 21, 479.

[11]. Julio A, Yu Shrike Z, Aleksander S, Ali K, Front. Bioeng. Biotechnol. Conference Abstract 2016, DOI: 10.3389/conf.FBIOE.2016.01.02158.

[12]. Pugno NM, Appl. Phys. Lett 2007, 90, 121918.

[13]. Hickey R, Ml L, Harden J, Pelling A, bioRxiv 2020, DOI: 10.1101/2020.11.06.371278.

[14]. Yang SY, O'Cearbhaill ED, Sisk GC, Park KM, Cho WK, Villiger M, Bouma BE, Pomahac B, Karp JM, Nat. Commun 2013, 4, 1702. [PubMed: 23591869]

[15]. Lee C, Kim SM, Kim YJ, Choi YW, Suh K-Y, Pang C, Choi M, ACS Appl. Mater. Interfaces 2015, 7, 2561. [PubMed: 25615547]

[16]. Fischer SCL, Levy O, Kroner E, Hensel R, Karp JM, Arzt E, J. Mech. Behav. Biomed. Mater 2016, 61, 87. [PubMed: 26849031]

[17]. Nichol JW, Khademhosseini A, Soft Matter 2009, 5, 1312. [PubMed: 20179781]

[18]. Xiao W, Xi H, Li J, Wei D, Li B, Liao X, Fan H, Mater. Lett 2018, 228, 360.

[19]. Bajaj P, Schweller RM, Khademhosseini A, West JL, Bashir R, Ann. Rev. Biomed. Eng 2014, 16, 247. [PubMed: 24905875]

[20]. Fernández-Pérez J, Kador KE, Lynch AP, Ahearne M, Mater. Sci. Eng. C Mater. Biol. Appl 2020, 108, 110415. [PubMed: 31924032]

[21]. Hurd SA, Bhatti NM, Walker AM, Kasukonis BM, Wolchok JC, Biomaterials 2015, 49, 9. [PubMed: 25725550]

[22]. Tonndorf R, Gossla E, Kocaman RT, Kirsten M, Hund R-D, Hoffmann G, Aibibu D, Gelinsky M, Cherif C, Text. Res. J 2018, 88, 1965.

[23]. Walther A, Hoyer B, Springer A, Mrozik B, Hanke T, Cherif C, Pompe W, Gelinsky M, Materials 2012, 5, 540. [PubMed: 28817062]

[24]. Steck E, Bertram H, Walther A, Brohm K, Mrozik B, Rathmann M, Merle C, Gelinsky M, Richter W, Tissue Eng. Part A 2010, 16, 3697. [PubMed: 20673020]

[25]. Hwang CM, Park Y, Park JY, Lee K, Sun K, Khademhosseini A, Lee SH, Biomed. Microdevices 2009, 11, 739. [PubMed: 19242806]

[26]. McCarthy A, John JV, Saldana L, Wang H, Lagerstrom M, Chen S, Su Y, Kuss M, Duan B, Carlson MA, Xie J, Adv. Healthcare Mater 2021, 2100766.

[27]. Gossla E, Bernhardt A, Tonndorf R, Aibibu D, Cherif C, Gelinsky M, Int. J. Mol. Sci 2021, 22, 9341. [PubMed: 34502249]

[28]. da Silva D, Kaduri M, Poley M, Adir O, Krinsky N, Shainsky-Roitman J, Schroeder A, Chem. Eng. J 2018, 340, 9. [PubMed: 31384170]

[29]. Araque-Monrós MC, Vidaurre A, Gil-Santos L, Gironés Bernabé S, Monleón-Pradas M, Más-Estellés J, Polymer Degrad. Stab 2013, 98, 1563.

[30]. McCarthy A, Shah R, John JV, Brown D, Xie J, Appl. Phys. Rev 2021, 8, 041326. [PubMed: 35003482]

[31]. Loening AM, James IE, Levenston ME, Badger AM, Frank EH, Kurz B, Nuttall ME, Hung HH, Blake SM, Grodzinsky AJ, Lark MW, Arch. Biochem. Biophys 2000, 381, 205. [PubMed: 11032407]

[32]. He R, Wang Z, Cui M, Liu S, Wu W, Chen M, Wu Y, Qu Y, Lin H, Chen S, Wang B, Shao Z, Autophagy 2021, 17, 3338. [PubMed: 33455530]

[33]. Takano-Yamamoto T, Jpn. Dent. Sci. Rev 2014, 50, 29–39.

[34]. Ramakrishnan O, Hecht B, Pedersen D, Lavery M, Maynard J, Buckwalter J, Martin J, J. Orthop. Res 2010, 28, 914. [PubMed: 20058262]

[35]. Valon L, Levayer R, Biol. Cell 2019, 111, 51. [PubMed: 30609052]

[36]. Sun B, Cell Rep. Phys. Sci 2021, 2, 100515. [PubMed: 34485951]

[37]. Frantz C, Stewart KM, Weaver VM, J. Cell Sci 2010, 123, 4195–4200. [PubMed: 21123617]

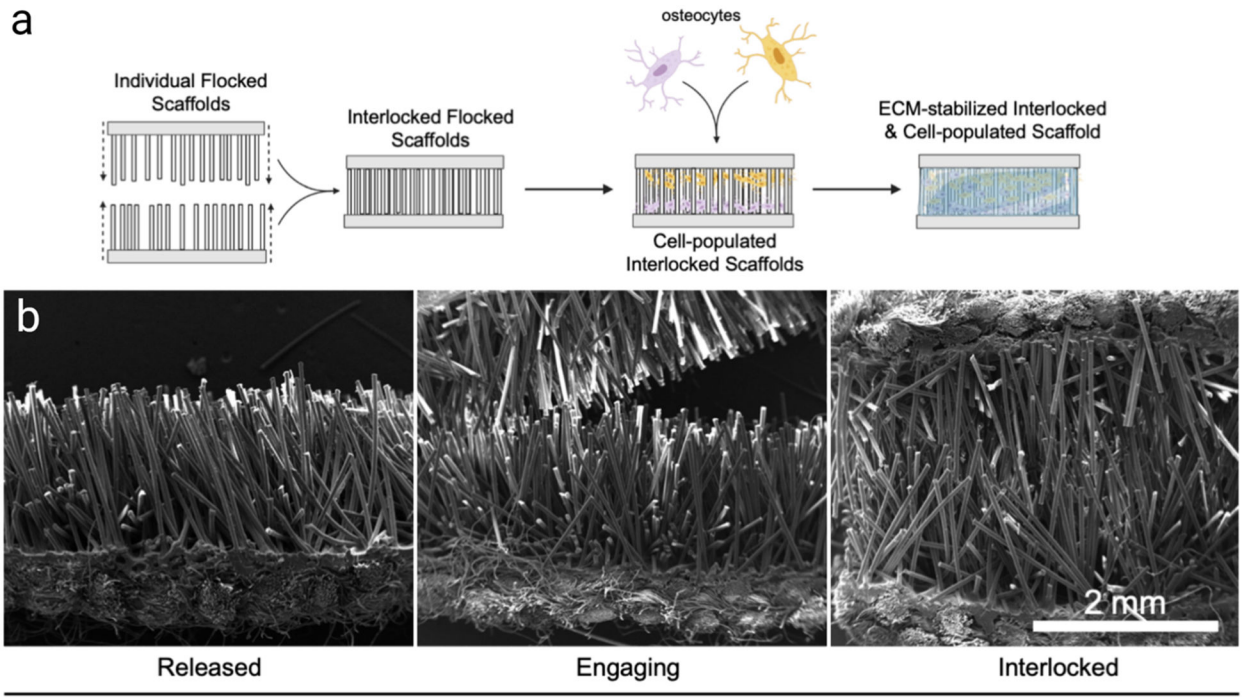

Figure 1.

Interlocking flocked scaffolds. (a) Schematic outline for the process of interlocking and reinforcing flocked scaffolds with osteocytes. (b) SEM images of released, engaging, and interlocked flocked scaffolds.

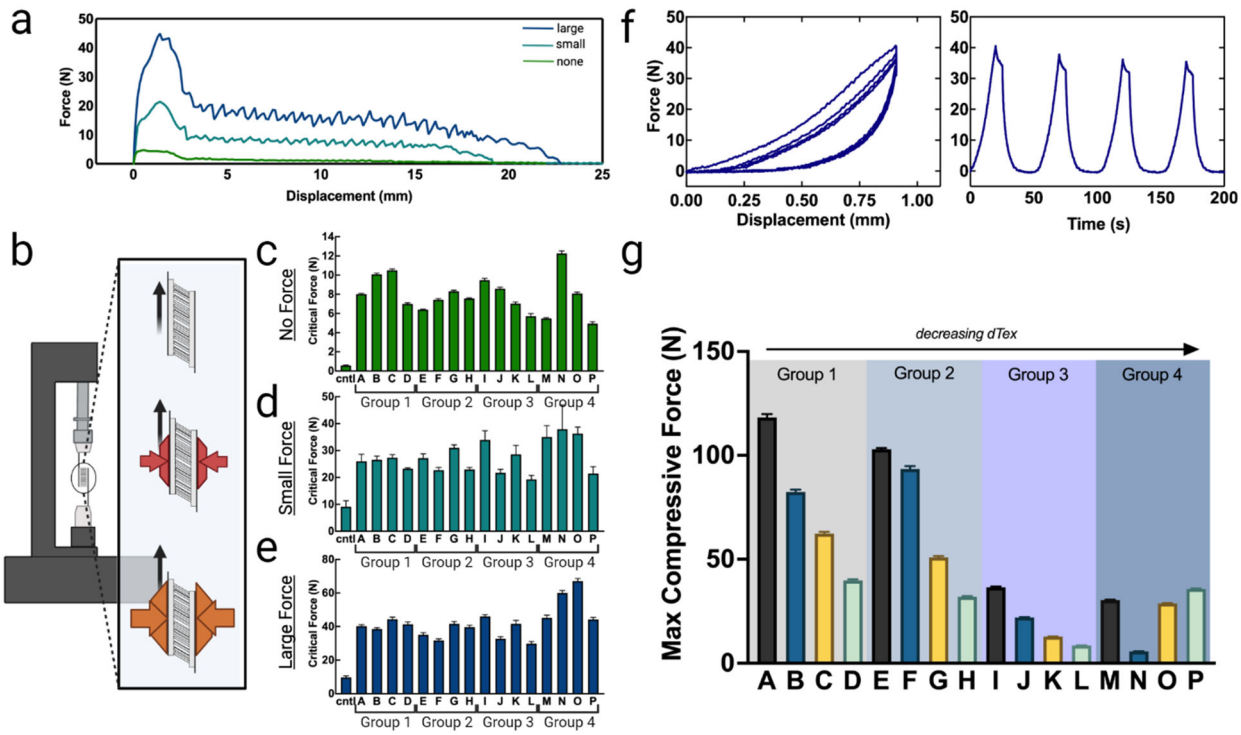

Figure 2.

Shearing and compression resistance of scaffolds A-P. (a) A representative shearing curve of scaffold P with a large, small, and no transverse load applied. (b) Schematic representation of transverse loading used in the modified tensile test. (c-e) Critical force graphs for scaffolds A-P under different transverse loads. (f) Representative hysteresis and compression curves for scaffold D. (g) Maximum compressive forces of scaffolds A-P. ($p < 0.0001$, n = 8). All summary p values are given in Tables S5-8. Each group represents the same dTex, while each colored bar graph represents the same fiber length.

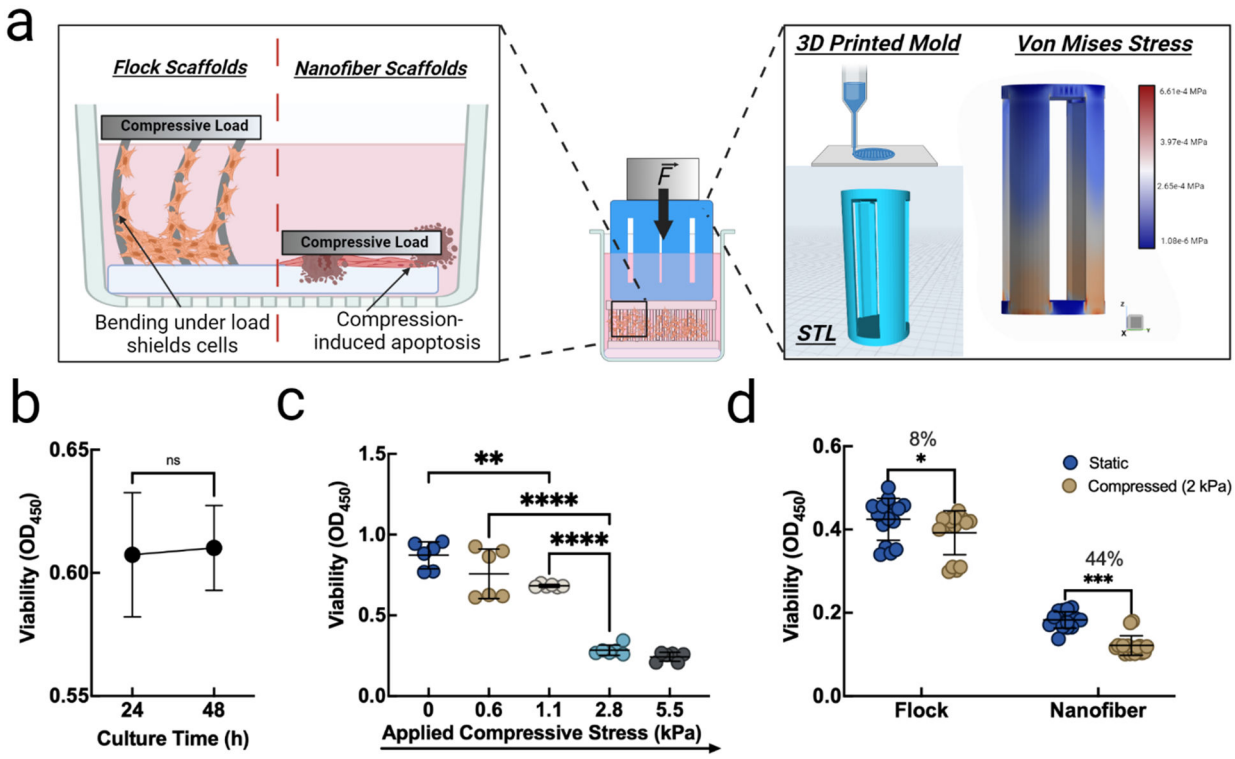

Figure 3.

Compression shielding of flocked scaffolds improves cell survivorship. (a) Proposed mechanism for protection against compression-induced apoptosis and STL and force distribution analysis of custom compression inserts. (b) Cytotoxicity analysis of 3D printed cell compression inserts. ($p = 0.827$, $n = 8$) (c) MC3T3-E1 cell viability under varying loads. (**$p < 0.05$, ****$p < 0.001$, $n = 8$) (d) Viability of static or compressed cells seeded on PLA flocked and electrospun scaffolds after 24 h. (*$p < 0.05$, ***$p < 0.001$, $n = 8$)

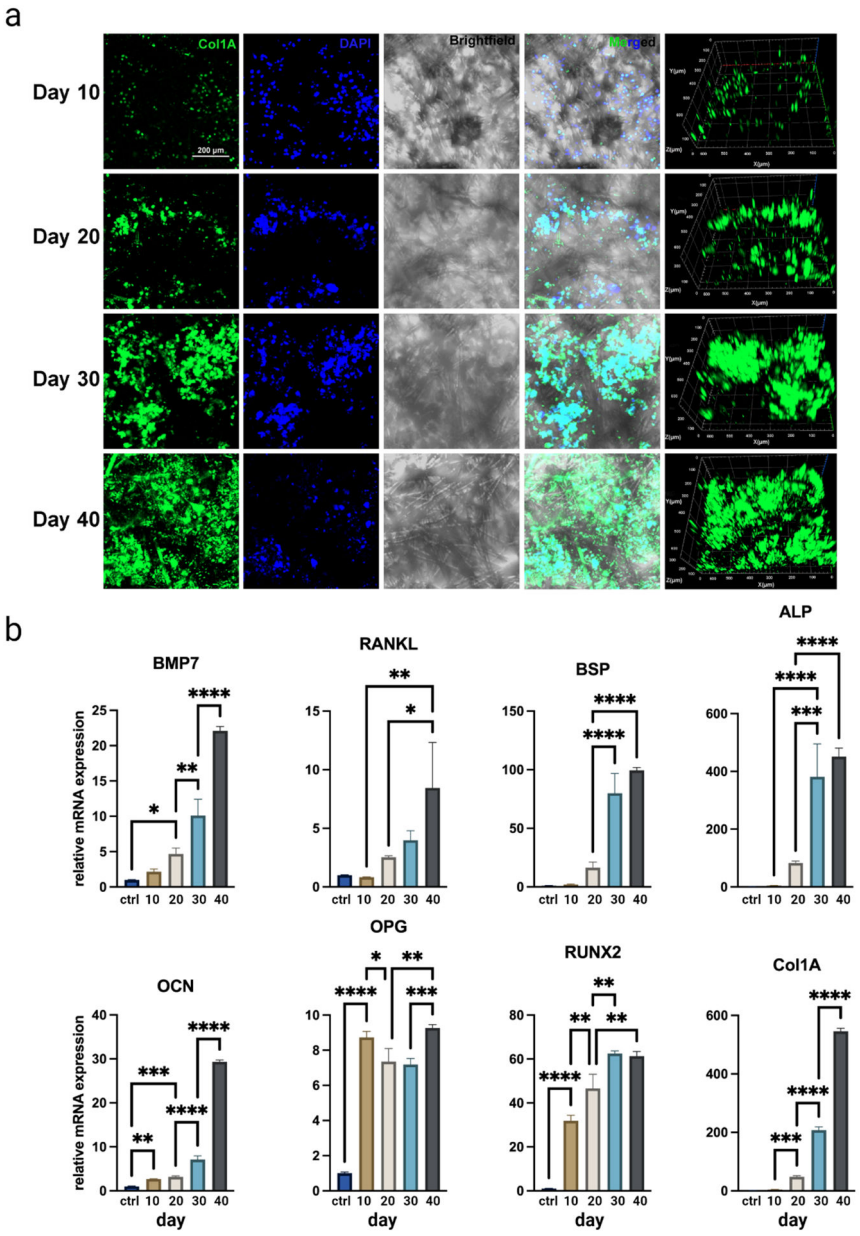

Figure 4.

Collagen-reinforced flocked scaffolds and cell viability and osteogenic differentiation. (a) Confocal staining of COL1A and DAPI on MC3T3-E1 cells-seeded interlocked scaffolds. (b) Protein expression of different hallmark osteogenic markers. (*$p < 0.05$, **$p < 0.01$, ***$p < 0.001$, ****$p < 0.0001$, n = 8)

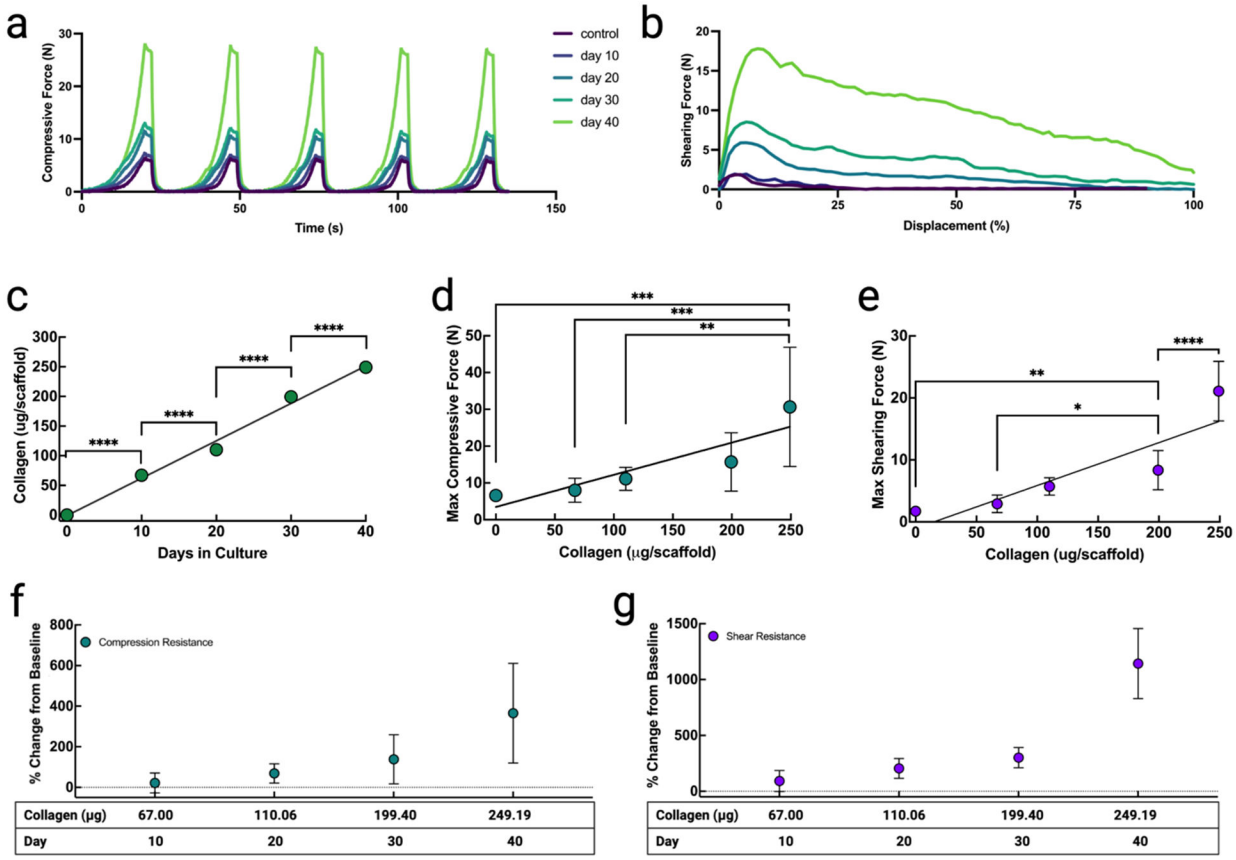

Figure 5.

Force curves of MC3T3-E1 cells-seeded interlocking scaffolds after culture for 10, 20, 30, and 40 days. (a) Compression resistance and (b) shearing resistance of interlocking scaffolds without (control) and with cell seeding for 10, 20, 30, and 40 days of culture. (c) Collagen content over 40 days of culture. (d) Correlation analysis of collagen content and compression resistance. (e) Correlation analysis of collagen content and maximum shearing resistance. (f) Percent change in compression and (g) shearing resistance relative to collagen content and culture time. (*p < 0.05, **p < 0.01, ***p < 0.001, ****p < 0.0001, n = 10)

Table 1.

Polyamide (Nylon 6,6) flock scaffold characteristics

Group	Sample	dTex	Length (μm)	Diameter(μm)	Max Orientation Frequency
1	A	25	500	52.46 ± 2.47	298.94
	B	25	750	48.55 ± 4.02	2178.86
	C	25	1000	52.76 ± 2.08	4832.12
	D	25	1500	52.89 ± 1.18	6165.80
2	E	15	500	44.98 ± 1.51	1684.60
	F	15	750	42.21 ± 1.48	2564.51
	G	15	1000	42.28 ± 1.85	2834.55
	H	15	1500	43.52 ± 2.17	2255.93
3	I	6	500	27.04 ± 1.70	4009.05
	J	6	750	27.47 ± 0.70	2410.88
	K	6	1000	27.55 ± 1.59	2430.41
	L	6	1500	28.47 ± 1.80	6143.42
4	M	3	50	19.10 ± 1.12	4064.11
	N	3	30	16.44 ± 2.56	2967.76
	O	1.5	30	16.00 ± 0.95	1944.62
	P	1.5	40	14.75 ± 0.59	4143.83